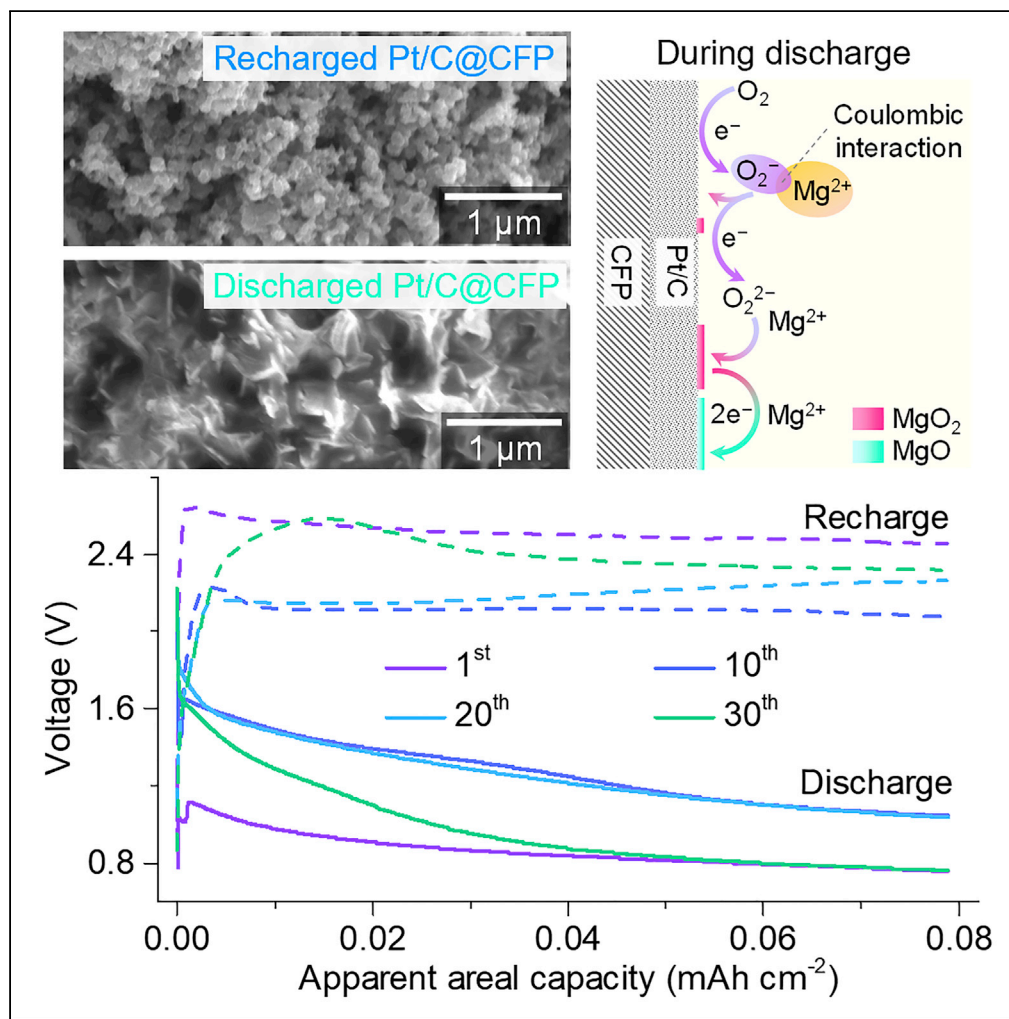


## Article

A rechargeable Mg|O<sub>2</sub> battery

Kok Long Ng,  
Kewei Shu, Gisele  
Azimi

g.azimi@utoronto.ca

#### Highlights

A rechargeable Mg|O<sub>2</sub> battery with prolonged cycle life (~35 cycles) is demonstrated

Mg((CF<sub>3</sub>SO<sub>2</sub>)<sub>2</sub>N)<sub>2</sub>-MgCl<sub>2</sub> in G2 enables reversible battery cycling O<sub>2</sub> environment

A multistep discharge product formation pathway is proposed

MgO is identified as the main discharge product

## Article

A rechargeable Mg|O<sub>2</sub> batteryKok Long Ng,<sup>1</sup> Kewei Shu,<sup>2</sup> and Gisele Azimi<sup>1,2,3,\*</sup>

## SUMMARY

**Rechargeable Mg|O<sub>2</sub> batteries (RMOBs) offer several advantages over alkali metal-based battery systems owing to Mg's ease of transport/storage in ambient environment, low cost originating from its high abundance, as well as the high theoretical specific energy of RMOBs. However, research on RMOBs has been stagnant for the past decade, largely owing to unacceptably poor electrochemical performance. Here, we present a RMOB that employs Mg anode, Mg((CF<sub>3</sub>SO<sub>2</sub>)<sub>2</sub>N)<sub>2</sub>-MgCl<sub>2</sub> in diglyme (G2) electrolyte, and commercial Pt/C on carbon fiber paper (Pt/C@CFP) oxygen cathode. This battery demonstrates unparalleled improvement over existing RMOBs by rendering a discharge capacity over 1.6 mAh cm<sup>-2</sup>, achieving cycle lives up to 35 cycles with a cumulative energy density of ~3.2 mWh cm<sup>-2</sup> at room temperature. This RMOB system seeks to reignite the pursuit of novel electrochemical systems based on Mg-O<sub>2</sub> chemistries.**

## INTRODUCTION

As the practical specific energy of commercial Li-ion batteries (LIBs) is approaching its limit, novel battery systems that can offer enhanced energy storage capabilities are greatly desired. To this end, metal|O<sub>2</sub> batteries have emerged as promising candidates due to their remarkably high theoretical specific energies. For instance, nonaqueous Li|O<sub>2</sub> batteries can deliver an ultrahigh theoretical specific energy of ~3456 Wh kg<sup>-1</sup> (assuming 2Li + O<sub>2</sub> ⇌ Li<sub>2</sub>O<sub>2</sub>), which is six times higher than that of commercial graphite|LiNi<sub>0.33</sub>Mn<sub>0.33</sub>Co<sub>0.33</sub>O<sub>2</sub> LIB (~575 Wh kg<sup>-1</sup>; Table S1). While calculations incorporating the mass contributions of non-electroactive components have led to a more modest estimate of the practical specific energy of Li|O<sub>2</sub> full cell (~610 Wh kg<sup>-1</sup>) (Kwak et al., 2020), nonetheless, this value is more than twice the practical limit of existing LIBs (~300 Wh kg<sup>-1</sup>). This desirable characteristic of metal|O<sub>2</sub> batteries has attracted substantial attention from researchers around the globe, leading to a drastic increase in research publications over the past few years (Liu et al., 2020). To date, various metal|O<sub>2</sub> battery systems employing alkali metals (Li, Na, and K), alkaline-earth metals (Mg and Ca), transition metals (Fe and Zn), and Al as the anode have been reported (Wang and Xu, 2019). In particular, Mg is an attractive anode material due to its relatively low cost, high capacities, high material abundance, and stability in ambient environment (Attias et al., 2019; Canepa et al., 2017; Mohtadi et al., 2021; Muldoon et al., 2017). Additionally, the theoretical specific energy of Mg|O<sub>2</sub> battery is among the highest (Table S1). These favorable properties prompted the research and development of primary Mg|O<sub>2</sub> batteries as early as the 1960s (Zhang et al., 2014).

Despite decades of study on primary Mg|O<sub>2</sub> batteries, only a handful of works explored rechargeable Mg|O<sub>2</sub> batteries (RMOBs) (Dong et al., 2016; Shiga et al., 2013, 2014; Vardar et al., 2015). The first report was by Shiga et al., in 2013, who utilized I<sup>2</sup>/I<sup>-</sup> couple as a redox mediator in Mg(ClO<sub>4</sub>)<sub>2</sub>-dimethylsulfoxide (DMSO) electrolyte (Shiga et al., 2013). The battery delivered an initial discharge capacity of 2131 mAh g<sup>-1</sup><sub>cathode</sub> at 60°C, but suffered severe capacity fading that led to limited rechargeability (~4 cycles). In the following studies, the performance of reported systems remained largely unsatisfactory (Table S2) (Dong et al., 2016; Shiga et al., 2014; Vardar et al., 2015). Given the inferior rechargeability, it is indicated that certain system(s) above should be considered as primary Mg|O<sub>2</sub> batteries (Gelman et al., 2019). One factor that leads to the limited rechargeability of Mg|O<sub>2</sub> batteries can be attributed to the passivation of electrodes. At the Mg anode, anions (e.g., ClO<sub>4</sub><sup>-</sup> and (CF<sub>3</sub>SO<sub>2</sub>)<sub>2</sub>N<sup>-</sup>) in single-salt Mg electrolytes are known to react with Mg metal to form an ionically insulating surface film, which drastically hinders subsequent Mg electroplating/stripping reactions (Lu et al., 1999; Rajput et al., 2015; Shimokawa et al., 2018). In addition, many polar aprotic solvents for nonaqueous electrochemistry (e.g., carbonates, nitriles, and lactones) are (electro)chemically incompatible with Mg metal (Attias et al., 2019). Similarly, these solvents react with Mg metal and form a passivating film that renders the electrode inactive. At

<sup>1</sup>Department of Materials Science and Engineering, University of Toronto, 184 College Street, Toronto, ON M5S 3E4, Canada

<sup>2</sup>Department of Chemical Engineering and Applied Chemistry, University of Toronto, 200 College Street, Toronto, ON M5S 3E5, Canada

<sup>3</sup>Lead contact

\*Correspondence: g.azimi@utoronto.ca  
<https://doi.org/10.1016/j.isci.2022.104711>



the oxygen cathode, incomplete/partial decomposition of discharge product (e.g., MgO and/or MgO<sub>2</sub>) represents another factor that can negatively affect the rechargeability of Mg|O<sub>2</sub> batteries (Shiga et al., 2014; Vardar et al., 2015).

To mitigate electrode passivation, the addition of Cl-containing salts can be an effective strategy. For instance, additions of MgCl<sub>2</sub> have been reported to markedly enhance Mg electrodeposition/stripping reactions in Mg((CF<sub>3</sub>SO<sub>2</sub>)<sub>2</sub>N)<sub>2</sub>-containing etheral electrolytes (Sa et al., 2016; Shimokawa et al., 2018; Shterenberg et al., 2015). It has been suggested that the addition of MgCl<sub>2</sub> minimizes unintended side reactions of Mg anode with trace H<sub>2</sub>O and/or (CF<sub>3</sub>SO<sub>2</sub>)<sub>2</sub>N<sup>-</sup> anions through the preferential adsorption of Cl-containing species on Mg surface (Connell et al., 2016), and at the same time, contributes to the formation of deposition-active Mg-Cl complex species in the electrolytes (Sa et al., 2016; Shimokawa et al., 2018). In addition, Cl-containing species in the electrolyte are known to facilitate the dissolution or breakdown of passivating Mg-O films (Attias et al., 2019; Wetteland et al., 2018), which is expected to accelerate the decomposition of discharge product (Mg oxide) on oxygen cathode during charging. It is worth mentioning that corrosion-resistant components should be used to prevent/avoid unintended corrosion of battery components in chloride-containing electrolytes (Tutusaus et al., 2015; Zhao-Karger et al., 2018). On the other hand, analogous to other nonaqueous alkali metal|O<sub>2</sub> batteries, oxygen reduction reaction (ORR) represents the initial electrochemical step during discharge of nonaqueous Mg|O<sub>2</sub> batteries (Reinsberg et al., 2016; Smith et al., 2016; Vardar et al., 2015, 2016). Among all, noble metal-based electrocatalysts are well known for their exceptional activity for ORR in aqueous and nonaqueous metal|O<sub>2</sub> batteries (Wang et al., 2014). The introduction of noble metal-based materials as air catalysts can be expected to facilitate ORR, thereby elevating the discharge voltage of resulting Mg|O<sub>2</sub> batteries.

In this work, we report a RMOB consisting of Mg anode, Mg((CF<sub>3</sub>SO<sub>2</sub>)<sub>2</sub>N)<sub>2</sub>-MgCl<sub>2</sub> in diglyme (G2) electrolyte, and commercially available Pt/C on carbon fiber paper (Pt/C@CFP) oxygen cathode. The battery rendered a full discharge capacity over 1.6 mAh cm<sup>-2</sup> and achieved a cycle life up to 35 cycles under a cut-off capacity of 0.08 mAh cm<sup>-2</sup> at 0.016 mA cm<sup>-2</sup>. A comprehensive characterization reveals reversible formation/dissolution of discharge product on Pt/C@CFP oxygen cathode during discharging/charging. The MgO is identified as the main discharge product and a multistep (electro)chemical pathway that leads to the formation of MgO is proposed.

## RESULTS

### Electrochemical properties of electrolyte

As discussed, the development of a suitable electrolyte that can enable reversible Mg deposition on metal anode while exhibiting enhanced oxidative and reductive stability represents one of the existing challenges faced by the field. For RMOBs, the challenge is further intensified through the involvement of O<sub>2</sub> in the electrochemistry. Many existing Mg electrolytes, such as Mg organohaloaluminate and all-inorganic MgCl<sub>2</sub>-AlCl<sub>3</sub> complex electrolytes, are air/moisture sensitive (He et al., 2017; Yagi et al., 2014). Furthermore, the high volatility of commonly employed organic solvents, such as tetrahydrofuran (THF) and dimethoxyethane (DME) (Table S3), further restricts the selection of suitable solvents for RMOB applications. To date, etheral solvents (e.g., glymes) are the only known family of polar, aprotic organic solvents that is thermodynamically compatible with Mg metals (Attias et al., 2019). Moreover, glymes are known for their profound stability toward ORR intermediates (e.g., O<sub>2</sub><sup>-</sup>) produced upon discharge at oxygen cathodes (Bryantsev et al., 2011, 2013; Schwenke et al., 2013). Herein, we report 0.5 m (Mg((CF<sub>3</sub>SO<sub>2</sub>)<sub>2</sub>N)<sub>2</sub>)<sub>2</sub> + 0.25 m MgCl<sub>2</sub> in G2 as a promising electrolyte for RMOB. Diglyme (G2) was preferred over other glymes because of its reasonably low volatility and viscosity (Table S3). The molar stoichiometric of Mg((CF<sub>3</sub>SO<sub>2</sub>)<sub>2</sub>N)<sub>2</sub>:MgCl<sub>2</sub> (= 2:1) used in this work was primarily referenced from the work by Sa et al. (2016) and Yoo et al. (2017). This particular Mg((CF<sub>3</sub>SO<sub>2</sub>)<sub>2</sub>N)<sub>2</sub>:MgCl<sub>2</sub> stoichiometry and the corresponding concentration (0.5 M Mg((CF<sub>3</sub>SO<sub>2</sub>)<sub>2</sub>N)<sub>2</sub> + 0.25 M MgCl<sub>2</sub> in G2) demonstrates the highest Mg plating/stripping coulombic efficiency while demonstrating low overpotentials (Sa et al., 2016).

Cyclic voltammetry was employed to investigate Mg deposition/stripping in Mg((CF<sub>3</sub>SO<sub>2</sub>)<sub>2</sub>N)<sub>2</sub>-MgCl<sub>2</sub> in G2 electrolyte (Figure 1A). Appreciable cathodic currents are observed at -0.5 V (vs. Mg) upon the negative scan, indicating Mg deposition, while the positive scan is characterized by a large oxidation peak, beginning at ~0 V, signaling Mg stripping reaction. In addition, this electrolyte displays reasonable oxidative stability of up to ~3.9 V (vs. Mg) on W working electrode (Figure 1B). This oxidative stability limit is in agreement with other binary Mg((CF<sub>3</sub>SO<sub>2</sub>)<sub>2</sub>N)<sub>2</sub>-MgCl<sub>2</sub> in glyme solutions of similar compositions (e.g., oxidative

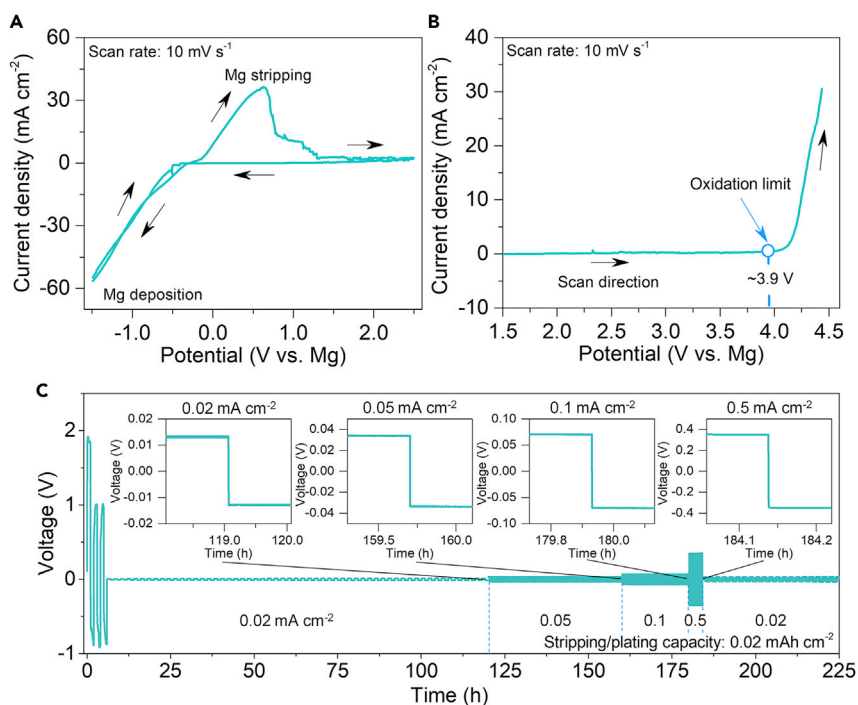


**Figure 1. Electrochemical performance of 0.5 m Mg((CF<sub>3</sub>SO<sub>2</sub>)<sub>2</sub>N)<sub>2</sub> + 0.25 m MgCl<sub>2</sub> in G2 electrolyte**

(A) Cyclic voltammogram of the electrolyte within the potential range between -1.5 and 2.5 V (vs. Mg) at 10 mV s<sup>-1</sup>.

(B) Linear sweep voltammogram of the electrolyte scanning from 1.5 to 4.4 V (vs. Mg) at 10 mV s<sup>-1</sup>.

(C) Galvanostatic stripping/plating of Mg-Mg symmetrical cell across various areal current densities with the areal capacity fixed at 0.02 mAh cm<sup>-2</sup>.

stability limits for 0.5 M Mg((CF<sub>3</sub>SO<sub>2</sub>)<sub>2</sub>N)<sub>2</sub> + 0.25 M MgCl<sub>2</sub> in monoglyme, and 0.5 M Mg((CF<sub>3</sub>SO<sub>2</sub>)<sub>2</sub>N)<sub>2</sub> + 0.25 M MgCl<sub>2</sub> in tetraglyme, were reported as 4.2 ± 0.4 V and 4.6 ± 0.2 V, respectively (Küpers et al., 2020). It is critical to point out that the oxidative stability determined using voltammetry-based techniques is sensitive to experimental variables such as the scan rate, cut-off current density, the nature and inertness of working electrodes, as well as the interaction between the electrolyte and the working electrode (Couston et al., 2017). To achieve more practically relevant conditions, the same metal (Mo) was utilized as the working electrode as well as the anode and cathode current collectors in determining oxidative stability limit of the electrolyte and in full Mg|O<sub>2</sub> batteries.

The long-term Mg deposition/stripping behavior was further evaluated via chronopotentiometry using a symmetrical Mg|Mg cell at a fixed areal capacity of 0.02 mAh cm<sup>-2</sup> (Figure 1C). In the initial few cycles, large Mg plating/stripping overpotentials are observed. This significant transition in Mg stripping/plating overpotentials with cycling maybe attributed to soft-shortening (Ding et al., 2018; Eaves-Rathert et al., 2020), reconstruction of the Mg-electrolyte interface that lowers interfacial resistance with cycling (Tutusaus et al., 2017), and/or unintended contamination on the surface of Mg electrodes during preparation (e.g., Mg electrodes were mechanically cleaned using a stainless-steel spatula to remove intrinsic magnesium oxide/hydroxide formed on the surface, and (re-)passivation of cleaned Mg electrodes due to high affinity with ambient O<sub>2</sub>, ~5 ppm of O<sub>2</sub>). Upon stabilization, symmetrical voltage profiles were observed and the corresponding overpotentials increased with increasing current density (within ± 0.4 V at current densities ≤ 0.5 mA cm<sup>-2</sup>). Noticeably, after testing of more than 200 h, Mg deposition/stripping reactions remain stable with an overpotential around ± 20 mV at 0.02 mA cm<sup>-2</sup>.

### Full-cell performance and analysis

Commercially available meshed CR2032 coin cells were used in the assembly of RMOBs in this work, and the cells were contained in O<sub>2</sub>-filled Swagelok bottles, as depicted in Figure 2A. The discharge-charge performance of RMOBs employing CFP and Pt/C@CFP oxygen cathodes is presented in Figure 2B. As expected, a significant improvement in terms of average discharge voltage ( $V_{avg}$ ; from 0.93 to 1.35 V) and

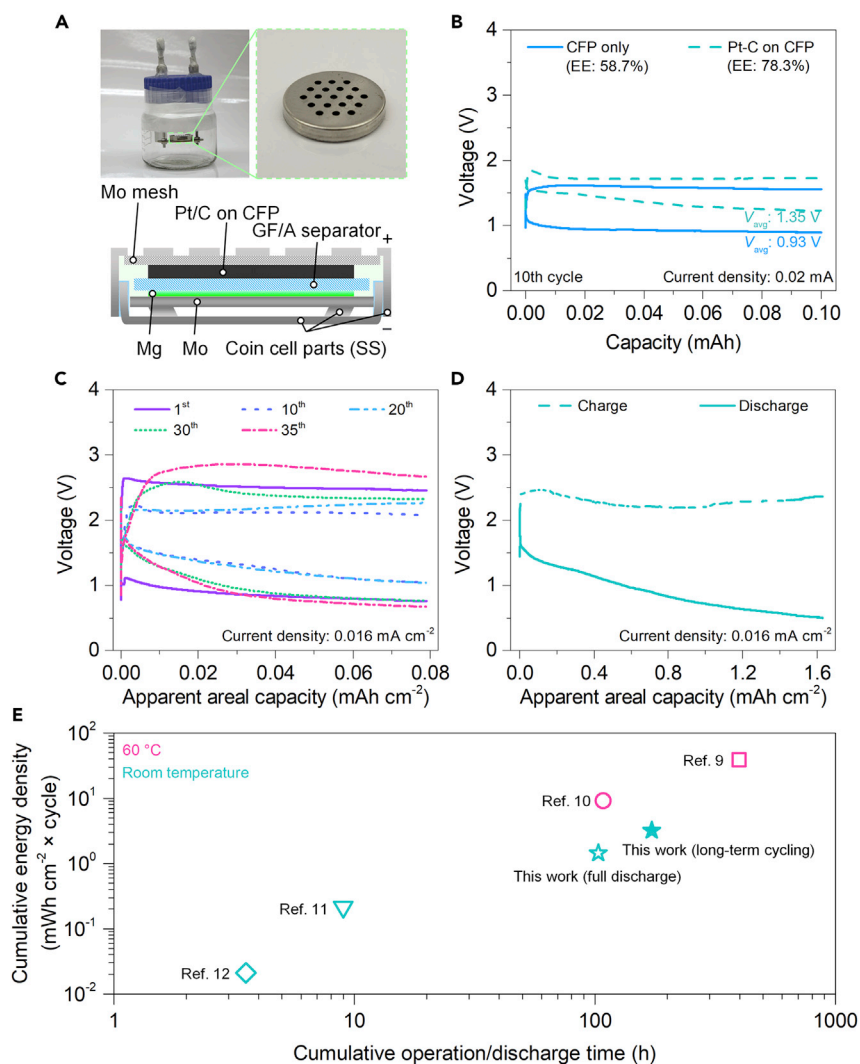


**Figure 2. Electrochemical performance of RMOB**

(A) Images of the assembled RMOB along with a schematic illustration of the inner construction of the cell.  
 (B) The 10<sup>th</sup> cycle voltage profiles of RMOB employing CFP only and Pt/C@CFP oxygen cathodes at an absolute current of 0.02 mA. (EE: Energy efficiency).  
 (C) Long-term cycling voltage profiles at 0.016 mA cm<sup>-2</sup>.  
 (D) Full discharge-charge voltage profile at 0.016 mA cm<sup>-2</sup> and 0.5 V discharge cut-off voltage.  
 (E) A plot compares the cumulative energy density and the cumulative operation/discharge time of reported RMOB systems. Tabulated data are provided in [Table S2](#).

energy efficiency (EE; from 58.7% to 78.3%) is observed in the cell employing Pt/C@CFP oxygen cathode containing ~0.2 mg Pt/C. This corroborates the well-known catalytic properties of Pt that facilitate ORR. To verify the involvement of O<sub>2</sub> in the electrochemical reaction, a separate cell was constructed with the inner atmosphere comprised of Ar. Under inert atmosphere, the cell exhibited no/negligible initial discharge capacity ([Figure S1](#)). When the inner atmosphere was replaced with O<sub>2</sub>, a similar discharge-charge voltage profile, analogous to that presented in [Figure 2B](#), was obtained. This further substantiates the critical role of O<sub>2</sub> in enabling electrochemical reactions in the developed battery.

To provide a more comprehensive assessment of cell performance, galvanostatic discharge-charge tests were conducted and the results are presented in [Figures 2C](#) and [2D](#). At a cut-off capacity of 0.08 mAh cm<sup>-2</sup>, the cell can run up to 35 cycles while maintaining V<sub>avg</sub> of ~0.92 V in the 35<sup>th</sup> cycle at 0.016 mAh cm<sup>-2</sup>. In addition, the cell achieved a full discharge capacity of 1.63 mAh cm<sup>-2</sup> with V<sub>avg</sub> of

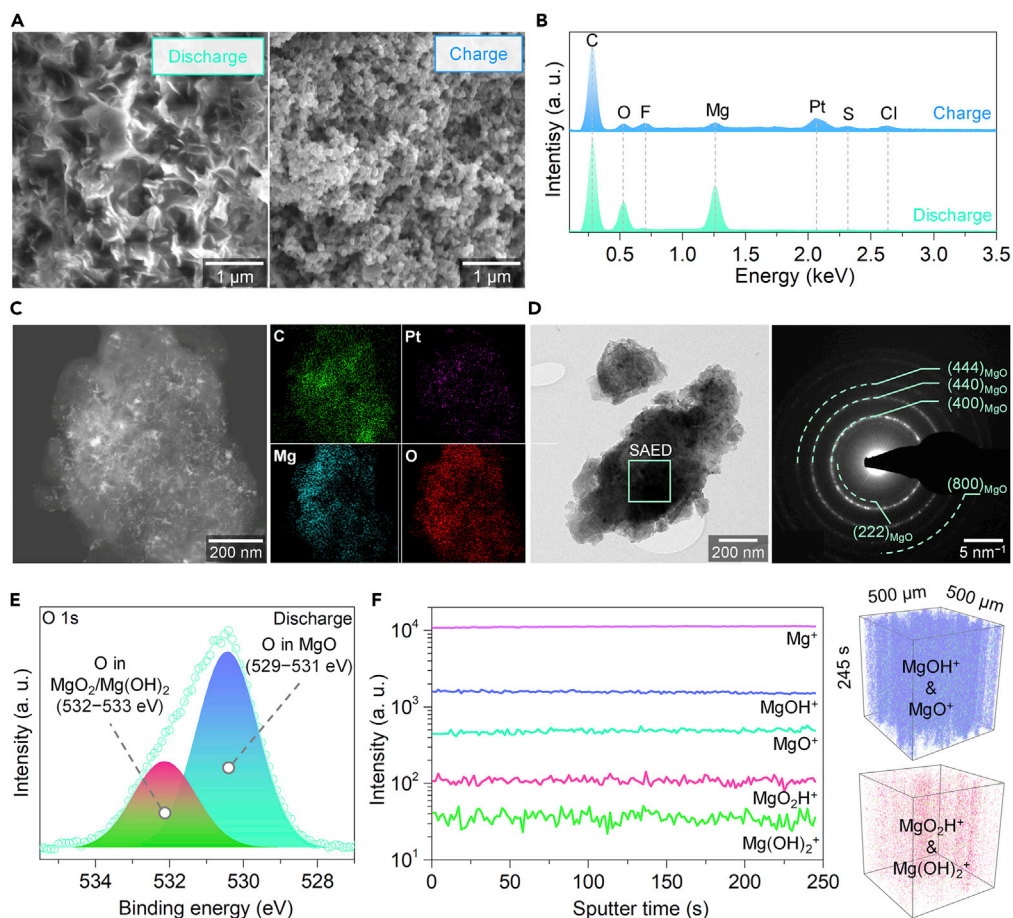


**Figure 3. Characterization of discharge product on Pt/C@CFP oxygen cathode**

- (A) Secondary electron images of discharged and charged electrodes.  
 (B) Corresponding energy dispersive spectra of discharged and charged electrodes.  
 (C) TEM dark-field image and elemental mapping of the discharge product.  
 (D) TEM bright-field image and the corresponding SAED pattern of the discharge product.  
 (E) XPS O 1s spectrum of the discharged electrode.  
 (F) ToF-SIMS results of the discharged electrode showing the intensity of various secondary ions as a function of sputtering time (left) and the corresponding 3D spatial distribution of  $\text{MgOH}^+$ ,  $\text{MgO}$ ,  $\text{MgO}_2\text{H}^+$ , and  $\text{Mg(OH)}_2^+$ .

$\sim 0.89$  V. To standardize the assessment of battery performance, the cumulative energy density ( $E_{\text{cum}}$ ) and cumulative operation/discharge time ( $t_{\text{cum}}$ ) of reported RMOB systems are presented in Figure 2E. The  $E_{\text{cum}}$  and  $t_{\text{cum}}$  achieved by the RMOB developed in this work ( $3.2 \text{ mWh cm}^{-2}$  and 173 h, respectively) are approximately 1–2 orders of magnitude higher compared with other RMOBs at room temperature (Dong et al., 2016; Vardar et al., 2015). These values are highly comparable with those obtained by Shiga et al. at  $60^\circ\text{C}$  (Shiga et al., 2013, 2014), which may be considered as primary batteries (Gelman et al., 2019).

### Characterization of discharge products and formation mechanism

Analogous to other rechargeable alkali metal| $\text{O}_2$  batteries, the formation of Mg-O compounds was expected on Pt/C@CFP oxygen cathodes upon discharge. Indeed, the surface of the discharged electrode was covered in a layer of Mg-O-rich compounds (Figures 3A and 3B). Upon charge, the layer disappeared, and the resulting surface morphology was visually identical to that of the pristine Pt/C air catalyst (Figure S2A). These observations also agreed with the results obtained from electrochemical impedance spectroscopy (EIS) studies presented in Figure S3. Notably, the resistance assigned to the discharge product,  $R_{\text{DP}}$ , was approximately 10 times higher in the discharged electrode ( $\sim 436 \text{ k}\Omega$ ) compared with that of the charged electrode ( $\sim 42.9 \text{ k}\Omega$ ; Figure S3A and Table S4). The high  $R_{\text{DP}}$ , along with the charge-up effects observed in the secondary electron image presented in Figure 3A, unequivocally indicate the poor

conducting nature of the discharge product layer. It is noteworthy that the small shoulder observed in the low-frequency region of the Bode plot ( $\sim 10^0 - 10^1$  Hz; Figure S3B) may indicate slightly incomplete dissociation of the discharge product upon charging, thus corroborating the weak Mg and O signals detected in the charged electrode (Figure 3B).

Transmission electron microscopy (TEM) was performed to characterize the discharge product. Element mapping presented in Figure 3C reveals the high association between Mg and O on Pt/C catalyst. In addition, the characteristic ring patterns observed in the selected-area electron diffraction (SAED) suggest polycrystalline nature of the discharge product (Figure 3D). It is worth mentioning that these patterns were not originating from the Pt/C catalyst as it exhibits different SAED patterns (Figure S2B). The lattice spacings determined from the SAED patterns were in good agreement with the (222), (400), (440), (444), and (800) planes of MgO, revealing the presence of MgO in the discharge product. Not limited to TEM, characterization techniques that cover larger lateral analysis areas, such as X-ray photoelectron spectroscopy (XPS) and time-of-flight secondary-ion mass spectroscopy (ToF-SIMS), and X-ray diffraction (XRD), were also employed. As presented in Figure 3E, the O 1s spectrum of the discharged electrode demonstrates a strong peak at the lower binding energy region (529–531 eV) and a weaker peak at the higher binding energy region (532–533 eV), which can be associated with O in MgO and MgO<sub>2</sub>/Mg(OH)<sub>2</sub>, respectively (Lee et al., 2002). This is in line with the ToF-SIMS results, which detected multiple secondary ions (MgO<sup>+</sup>, MgOH<sup>+</sup>, MgO<sub>2</sub>H<sup>+</sup>, and Mg(OH)<sub>2</sub><sup>+</sup>) of MgO and MgO<sub>2</sub>/Mg(OH)<sub>2</sub> (Figure 3F). However, from the XRD pattern presented in Figure S3, Mg(OH)<sub>2</sub> represents the only identifiable phase in the discharged electrode. As the hydroxylation of MgO is spontaneous even under extremely low moisture content ( $10^{-6}$  atm H<sub>2</sub>O; Figure S5A), a considerable proportion of MgO likely hydrolyzed and formed Mg(OH)<sub>2</sub> during XRD data acquisition.

In view of thermodynamics (Table S5), the formation of superoxide ions ( $E^\circ(\text{O}_2/\text{O}_2^-) = 2.02\text{--}2.19$  V vs. Mg) is expected to precede that of peroxide ions ( $E^\circ(\text{O}_2/\text{O}_2^{2-}) = 0.78$  V). For this reason, analogous to alkali metal O<sub>2</sub> batteries, O<sub>2</sub>/O<sub>2</sub><sup>-</sup> ORR has been proposed as the initial electrochemical step, followed by chemical reactions between Mg<sup>2+</sup> and O<sub>2</sub><sup>-</sup> to form MgO<sub>2</sub>, and subsequently, disproportionation of MgO<sub>2</sub> into MgO ( $2\text{MgO}_2 = 2\text{MgO} + \text{O}_2$ ) (Vardar et al., 2015). However, it is critical to point out that the proposed MgO<sub>2</sub> disproportionation reaction may be nonspontaneous (Figure S5B). Moreover, ORR in aprotic solvents is known to be affected by the type of divalent cations present as well as the working electrode material (Reinsberg et al., 2018). In aprotic solvents containing Mg<sup>2+</sup> ions, O<sub>2</sub><sup>2-</sup> ions have been reported as the main ORR product on Pt and glassy carbon electrodes (Reinsberg et al., 2018). The authors suggest that the overall ratio of O<sub>2</sub><sup>2-</sup> to O<sub>2</sub><sup>-</sup> is higher in electrolytes containing strongly polarizing cations (e.g., Mg<sup>2+</sup> and Ba<sup>2+</sup>), as these ions accelerate the O<sub>2</sub><sup>-</sup> → O<sub>2</sub><sup>2-</sup> electron transfer reaction by withdrawing electron density from O<sub>2</sub><sup>-</sup>, while the rate of O<sub>2</sub><sup>-</sup> diffusion into the bulk electrolyte remains mostly unchanged (or lowered due to the interaction with the cations). Providing that Mg<sup>2+</sup> ions are also present in Mg((CF<sub>3</sub>SO<sub>2</sub>)<sub>2</sub>N)<sub>2</sub>-MgCl<sub>2</sub> in G2 electrolyte (Figure S6), we rationally anticipate a similar ORR behavior on Pt/C@CFP oxygen cathode during discharge. It is critical to emphasize that the relative abundance of speciation in Mg((CF<sub>3</sub>SO<sub>2</sub>)<sub>2</sub>N)<sub>2</sub>-MgCl<sub>2</sub> in glyme electrolyte solutions is strongly dependent on the molar ratio of Mg((CF<sub>3</sub>SO<sub>2</sub>)<sub>2</sub>N)<sub>2</sub> to MgCl<sub>2</sub> (Wróbel et al., 2020). At a higher MgCl<sub>2</sub> content (e.g., Mg((CF<sub>3</sub>SO<sub>2</sub>)<sub>2</sub>N)<sub>2</sub>:MgCl<sub>2</sub> = 1:1 by mole), Mg<sup>2+</sup> ions tend to form stable Mg-Cl complexes. However, at lower MgCl<sub>2</sub> content (e.g., Mg((CF<sub>3</sub>SO<sub>2</sub>)<sub>2</sub>N)<sub>2</sub>:MgCl<sub>2</sub> = 2:1), due to less Cl<sup>-</sup> than metal cations, a considerable amount of Mg<sup>2+</sup> ions is expected to be in equilibrium with complexes such as MgCl<sup>+</sup>, MgCl<sub>2</sub>, and Mg<sub>2</sub>Cl<sub>y</sub><sup>(4-y)+</sup> (y > 4) (Wróbel et al., 2020), as evidenced in Figure S6.

Based on the above characterization results along with existing knowledge, a reaction pathway during discharge of Mg|O<sub>2</sub> battery developed in this work is proposed (Figure 4). Upon discharge, O<sub>2</sub> is first electrochemically reduced to form O<sub>2</sub><sup>-</sup> on Pt/C@CFP oxygen cathode. The strong electrostatic interaction between Mg<sup>2+</sup> and O<sub>2</sub><sup>-</sup> facilitates the O<sub>2</sub><sup>-</sup> → O<sub>2</sub><sup>2-</sup> reduction reaction, resulting in a predominant abundance of O<sub>2</sub><sup>2-</sup> being generated at the electrode surface. Subsequently, MgO<sub>2</sub> is formed as the product of the chemical reaction of Mg<sup>2+</sup> with O<sub>2</sub><sup>2-</sup>. Instead of undergoing a disproportionate reaction, MgO<sub>2</sub> is expected to be electrochemically reduced to form MgO upon combining with Mg<sup>2+</sup> and acquiring two electrons from the external circuit, given the thermodynamic spontaneity of the reaction (Table S5). Through theoretical density functional theory (DFT) calculations, Smith et al. also demonstrated that multistep MgO formation pathway (first MgO<sub>2</sub>, and subsequently MgO) is energetically more favorable compared with single-step formation pathway ( $\text{Mg} + 1/2\text{O}_2 + 2\text{e}^{2-} = \text{MgO}$ ) on (100)<sub>MgO</sub> (Smith et al., 2016). It is worth mentioning that the DFT-computed limiting discharge potential via multistep pathway (1.15 V) is in good

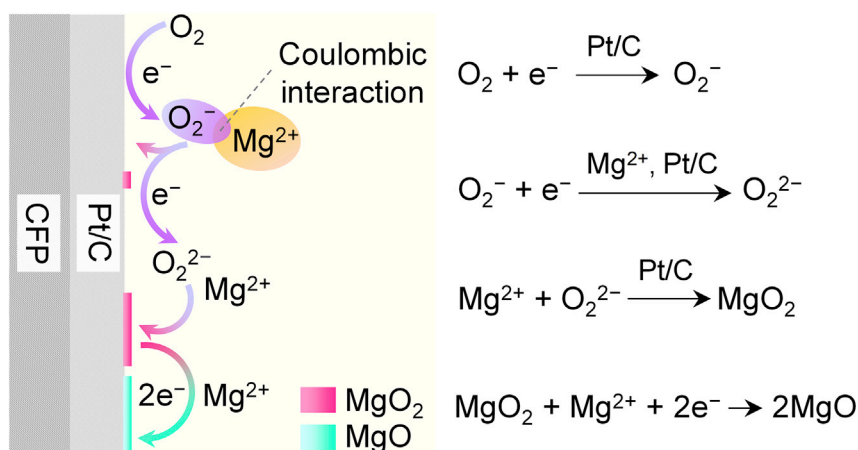
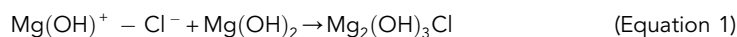


**Figure 4. Multistep discharge product formation pathway proposed in this work**

agreement with  $V_{\text{avg}}$  obtained in this work (0.89–1.35 V), but the predicted limiting charge potential (3.98 V) is substantially higher than the experimentally determined values (highest  $V_{\text{avg}}$  for charging:  $\sim 2.72$  V). As Cl-containing species are known to facilitate the breakdown of Mg-O compounds (Attias et al., 2019; Wetteland et al., 2018), such effect is expected to positively contribute to the dissolution of MgO (and MgO<sub>2</sub>) upon charging, leading to lower-than-predicted charge voltage and improved cyclability of RMOB developed in this work.

To investigate potential soluble species generated from the contact of MgO with the electrolyte, calcined/dried MgO (at 1000°C) powder was added into 0.5 m Mg((CF<sub>3</sub>SO<sub>2</sub>)<sub>2</sub>N)<sub>2</sub> + 0.25 m MgCl<sub>2</sub> in G2 electrolyte, and the mixture was allowed to equilibrate for several days at room temperature in the glovebox. The resulting supernatant was then extracted and the species in the supernatant was analyzed using Fourier transform mass spectrometry (FTMS). As illustrated in Figure S7, the MgO-soaked electrolyte contains several Mg-containing species that were not observed in the original electrolyte solution. This suggests new soluble species are being generated when MgO is in equilibrium with the chloride-containing electrolyte solution. The presence of Na-containing species in the electrolyte is likely due to the unintended ion exchange between the molecular sieves and the electrolyte solution. This artifact could be avoided by only treating pure D2 with molecular sieves, rather than the electrolyte solution.

In an aqueous solution, it has been suggested that Cl<sup>-</sup> could bind to the intermediate MgOH<sup>+</sup> formed during Mg(OH)<sub>2</sub> dissociation by forming Mg<sub>2</sub>(OH)<sub>3</sub>Cl species (Wetteland et al., 2018). Chloride ions are proposed to stabilize the charge in MgOH<sup>+</sup> species, which could reduce the adsorption of H<sup>+</sup> to nearby Mg(OH)<sub>2</sub>, thus promoting the dissociation of Mg(OH)<sub>2</sub> (Wetteland et al., 2018). A possible reaction route that can lead to the formation of Mg<sub>2</sub>(OH)<sub>3</sub>Cl in H<sub>2</sub>O-limiting environment is considered:



By investigating the Cl 2p binding energy on discharged and charged electrodes (Figure S8A), we noticed the discharged electrode exhibits a strong peak at  $\sim 197.4$  eV, which is not observed in the (re)charged electrode. The assignment of the exact Cl-containing species that show binding energy at this range is complicated by the lack of XPS binding energy data, as well as the presence of multiple Cl-containing species in the system (e.g., various Mg-Cl species). To identify this potential species, we looked into the ToF-SIMS spectrum of discharged Pt/C@CFP electrode in negative ion mode (Figure S8B). Detailed analysis of the spectrum confirms the formation of Mg<sub>2</sub>ClO<sub>3</sub>H<sub>4</sub><sup>-</sup> species on the discharged electrode. It is considered that rather than thermodynamically stable MgO, the dissolution of this Mg-O-Cl-H species may contribute to the lower-than-expected recharging voltage reported in this work. As evidenced in Figure S8C, the emergence of a tiny peak at  $\sim 72.8$  eV indicates the chlorination of Pt/C air catalyst in the discharged oxygen cathodes (sub Pt-C bond) (Kwon et al., 1998). Overall, the proportion of sub Pt-C bond remained low, and the chemical environment of discharged Pt remained similar to that of pristine Pt in Pt/C air catalyst. Given multiple species are present in the electrolyte as well as in the discharge product(s), the exact

mechanism involved in the recharging process is still unclear and requires further investigation in both theoretical and experimental research.

## DISCUSSION

To date, very limited studies have investigated rechargeable Mg|O<sub>2</sub> batteries (RMOBs) despite RMOBs harbor the potential of delivering higher theoretical specific energy, not to mention the various benefits of employing Mg as the anode material, including high natural abundance, low cost, and ease of handling in ambient conditions. One major factor that leads to the limited number of studies on RMOBs can be attributed to their poor electrochemical performance in terms of rechargeability and capacity, which renders their application impractical. In this study, we present a RMOB that demonstrates stable electrochemical performance over several tens of cycles owing to reversible electrochemistry at the electrodes. The employment of Pt/C@CFP oxygen cathode in combination with Mg((CF<sub>3</sub>SO<sub>2</sub>)<sub>2</sub>N)<sub>2</sub>-MgCl<sub>2</sub> in G2 electrolyte effectively overcomes electrode passivation issues that plagued prior works, leading to a substantial improvement in terms of rechargeability and discharge capacity. The improvement of battery performance can be rationally attributed to the multistep discharge product formation pathway, which is systematically corroborated by thermodynamic considerations along with integrated experimental evidence (SEM/TEM, XPS, ToF-SIMS, etc.).

## Limitations of the study

In this study as well in existing works on RMOBs, effective Mg utilization in full-cell configuration was not evaluated. The determination of effective Mg utilization in the cell is particularly important for the practical application of Mg|O<sub>2</sub> batteries, which undoubtedly deserves serious attention/investigation. In addition, the characterization of Mg anode, either in the Mg|O<sub>2</sub> battery or in the Mg symmetric cells, was also lacking. To gain more insights into the transition of Mg anode morphology with cycling, a controlled Mg preparation method and condition should be used to minimize unintended artifacts due to man-made experimental errors. In addition, extensive computational and experimental works are necessary to understand the mechanism/species responsible for the dissolution of discharge product(s) upon charging.

## SUPPORTING CITATIONS

(Aminabhavi and Gopalakrishna, 1995; Dong et al., 2016; Esch and Bredow, 2016; Fulem et al., 2011; Jain et al., 2013; Koppenol et al., 2010; Lodge et al., 2014; López and Ratner, 1996; Nitta et al., 2015; Pal and Singh, 1996; Scott, 1970; Shiga et al., 2013, 2014; Smith et al., 2016; Vardar et al., 2015).

## STAR★METHODS

Detailed methods are provided in the online version of this paper and include the following:

- **KEY RESOURCES TABLE**
- **RESOURCE AVAILABILITY**
  - Lead contact
  - Materials availability
  - Data and code availability
- **METHOD DETAILS**
  - Preparation of Mg((CF<sub>3</sub>SO<sub>2</sub>)<sub>2</sub>N)<sub>2</sub>-MgCl<sub>2</sub> in G2 electrolyte
  - Fabrication of Pt/C on CFP air cathode
  - Fabrication of electrochemical cells
  - Electrochemical testings and characterization
  - Calculations of theoretical  $E_{AM}$

## SUPPLEMENTAL INFORMATION

Supplemental information can be found online at <https://doi.org/10.1016/j.isci.2022.104711>.

## ACKNOWLEDGMENTS

The authors acknowledge the financial support provided by the University of Toronto CESeed Funding. The authors sincerely thank Robert Flick for his help with the Fourier-transform mass spectroscopy (FTMS).

data acquisition and analysis. The authors would like to thank Dr. Peter Broderson for his help with ToF-SIMS data acquisition and analysis.

## AUTHOR CONTRIBUTIONS

G.A. conceptualized the work. K.L.N. and K.S. conducted the experiments. K.L.N. constructed the manuscript. All authors (K.L.N., K.S., and G.A.) discussed, and revised the manuscript. K.L.N. and K.S. contributed equally to this work.

## DECLARATION OF INTERESTS

The authors declare no conflict of interest.

Received: March 28, 2022

Revised: May 31, 2022

Accepted: June 28, 2022

Published: August 19, 2022

## REFERENCES

- Aminabhavi, T.M., and Gopalakrishna, B. (1995). Density, viscosity, refractive index, and speed of sound in aqueous mixtures of *N,N*-dimethylformamide, dimethyl sulfoxide, *N,N*-dimethylacetamide, acetonitrile, ethylene glycol, diethylene glycol, 1, 4-dioxane, tetrahydrofuran. *J. Chem. Eng. Data* 40, 856–861.
- Attias, R., Salama, M., Hirsch, B., Goffer, Y., and Aurbach, D. (2019). Anode-electrolyte interfaces in secondary magnesium batteries. *Joule* 3, 27–52. <https://doi.org/10.1016/j.joule.2018.10.028>.
- Betz, J., Bieker, G., Meister, P., Placke, T., Winter, M., and Schmuch, R. (2019). Theoretical versus practical energy: a plea for more transparency in the energy calculation of different rechargeable battery systems. *Adv. Energy Mater.* 9, 1803170. <https://doi.org/10.1002/aenm.201803170>.
- Bryantsev, V.S., Giordani, V., Walker, W., Blanco, M., Zecevic, S., Sasaki, K., Uddin, J., Addison, D., and Chase, G.V. (2011). Predicting solvent stability in aprotic electrolyte Li-air batteries: nucleophilic substitution by the superoxide anion radical ( $O_2^{\cdot -}$ ). *J. Phys. Chem. A* 115, 12399–12409. <https://doi.org/10.1021/jp2073914>.
- Bryantsev, V.S., Uddin, J., Giordani, V., Walker, W., Addison, D., and Chase, G.V. (2013). The identification of stable solvents for nonaqueous rechargeable Li-air batteries. *J. Electrochem. Soc.* 160, A160–A171. <https://doi.org/10.1149/2.027302jes>.
- Canepa, P., Sai Gautam, G., Hannah, D.C., Malik, R., Liu, M., Gallagher, K.G., Persson, K.A., and Ceder, G. (2017). Odyssey of multivalent cathode materials: open questions and future challenges. *Chem. Rev.* 117, 4287–4341. <https://doi.org/10.1021/acs.chemrev.6b00614>.
- Connell, J.G., Genorio, B., Lopes, P.P., Strmcnik, D., Stamenkovic, V.R., and Markovic, N.M. (2016). Tuning the reversibility of Mg anodes via controlled surface passivation by  $H_2O/Cl^-$  in organic electrolytes. *Chem. Mater.* 28, 8268–8277. <https://doi.org/10.1021/acs.chemmater.6b03227>.
- Coustan, L., Shul, G., and Bélanger, D. (2017). Electrochemical behavior of platinum, gold and glassy carbon electrodes in water-in-salt electrolyte. *Electrochem. Commun.* 77, 89–92. <https://doi.org/10.1016/j.elecom.2017.03.001>.
- Ding, M.S., Diemant, T., Behm, R.J., Passerini, S., and Giffin, G.A. (2018). Dendrite growth in Mg metal cells containing  $Mg(TFSI)_2$ /glyme electrolytes. *J. Electrochem. Soc.* 165, A1983–A1990. <https://doi.org/10.1149/2.1471809jes>.
- Dong, Q., Yao, X., Luo, J., Zhang, X., Hwang, H., and Wang, D. (2016). Enabling rechargeable non-aqueous Mg–O<sub>2</sub> battery operations with dual redox mediators. *Chem. Commun.* 52, 13753–13756. <https://doi.org/10.1039/c6cc07818d>.
- Eaves-Rathert, J., Moyer, K., Zohair, M., and Pint, C.L. (2020). Kinetic- versus diffusion-driven three-dimensional growth in magnesium metal battery anodes. *Joule* 4, 1324–1336. <https://doi.org/10.1016/j.joule.2020.05.007>.
- Esch, T.R., and Bredow, T. (2016). Bulk and surface properties of magnesium peroxide  $MgO_2$ . *Appl. Surf. Sci.* 389, 1202–1207. <https://doi.org/10.1016/j.apsusc.2016.07.141>.
- Fulem, M., Růžicka, K., and Růžicka, M. (2011). Recommended vapor pressures for thiophene, sulfolane, and dimethyl sulfoxide. *Fluid Phase Equil.* 303, 205–216. <https://doi.org/10.1016/j.fluid.2011.02.002>.
- Gelman, D., Shvartsev, B., and Ein-Eli, Y. (2019). Challenges and prospect of non-aqueous non-alkali (NANA) metal-air batteries. In *Electrochemical Energy Storage*, pp. 127–168. [https://doi.org/10.1007/978-3-030-26130-6\\_5](https://doi.org/10.1007/978-3-030-26130-6_5).
- He, S., Luo, J., and Liu, T.L. (2017).  $MgCl_2/AlCl_3$  electrolytes for reversible Mg deposition/stripping: electrochemical conditioning or not? *J. Mater. Chem.* 5, 12718–12722. <https://doi.org/10.1039/c7ta01769c>.
- Jain, A., Ong, S.P., Hautier, G., Chen, W., Richards, W.D., Dacek, S., Cholia, S., Gunter, D., Skinner, D., Ceder, G., and Persson, K.A. (2013). Commentary: the materials project: a materials genome approach to accelerating materials innovation. *Apl. Mater.* 1, 011002. <https://doi.org/10.1063/1.4812323>.
- Kasavajjula, U., Wang, C., and Appleby, A.J. (2007). Nano- and bulk-silicon-based insertion anodes for lithium-ion secondary cells. *J. Power Sources* 163, 1003–1039. <https://doi.org/10.1016/j.jpowsour.2006.09.084>.
- Koppenol, W.H., Stanbury, D.M., and Bounds, P.L. (2010). Electrode potentials of partially reduced oxygen species, from dioxygen to water. *Free Radic. Biol. Med.* 49, 317–322. <https://doi.org/10.1016/j.freeradbiomed.2010.04.011>.
- Küpers, V., Weintz, D., Mück-Lichtenfeld, C., Bieker, P., Winter, M., and Kolek, M. (2020). Approaching electrochemical limits of  $Mg_xCl_y^{z+}$  complex-based electrolytes for Mg batteries by tailoring the solution structure. *J. Electrochem. Soc.* 167, 160505. <https://doi.org/10.1149/1945-7111/abc7e4>.
- Kwak, W.J., Sharon, D., Xia, C., Kim, H., Johnson, L.R., Bruce, P.G., Nazar, L.F., Sun, Y.K., Frimer, A.A., et al. (2020). Lithium–oxygen batteries and related systems: potential, status, and future. *Chem. Rev.* 120, 6626–6683. <https://doi.org/10.1021/acs.chemrev.9b00609>.
- Kwon, K.-H., Kim, C.-I., Yun, S.J., and Yeom, G.-Y. (1998). Etching properties of Pt thin films by inductively coupled plasma. *J. Vac. Sci. Technol. A Vacuum, Surfaces, Film* 16, 2772–2776. <https://doi.org/10.1116/1.581420>.
- Lee, S.M., Ito, T., and Murakami, H. (2002). X-ray photoelectron spectroscopy characterization and morphology of  $MgO$  thin films grown on single-crystalline diamond (100). *J. Mater. Res.* 17, 1914–1922. <https://doi.org/10.1557/JMR.2002.0284>.
- Liu, Q., Pan, Z., Wang, E., An, L., and Sun, G. (2020). Aqueous metal-air batteries: fundamentals and applications. *Energy Storage Mater.* 27, 478–505. <https://doi.org/10.1016/j.ensm.2019.12.011>.
- Lodge, A.W., Lacey, M.J., Fitt, M., Garcia-Araez, N., and Owen, J.R. (2014). Critical appraisal on the role of catalysts for the oxygen reduction reaction in lithium-oxygen batteries. *Electrochim. Acta* 140, 168–173. <https://doi.org/10.1016/j.electacta.2014.05.026>.

- López, G.P., and Ratner, B.D. (1996). Molecular adsorption and the chemistry of plasma-deposited thin organic films: deposition of oligomers of ethylene glycol. *Plasma Polym. 1*, 127–151. <https://doi.org/10.1007/BF02532823>.
- Lu, Z., Schechter, A., Moshkovich, M., and Aurbach, D. (1999). On the electrochemical behavior of magnesium electrodes in polar aprotic electrolyte solutions. *J. Electroanal. Chem.* 466, 203–217. [https://doi.org/10.1016/S0022-0728\(99\)00146-1](https://doi.org/10.1016/S0022-0728(99)00146-1).
- Mohtadi, R., Tutasaus, O., Arthur, T.S., Zhao-Karger, Z., and Fichtner, M. (2021). The metamorphosis of rechargeable magnesium batteries. *Joule* 5, 581–617. <https://doi.org/10.1016/j.joule.2020.12.021>.
- Muldoon, J., Bucur, C.B., and Gregory, T. (2017). Fervent hype behind magnesium batteries: an open call to synthetic chemists—electrolytes and cathodes needed. *Angew. Chem. Int. Ed.* 56, 12064–12084. <https://doi.org/10.1002/anie.201700673>.
- Nitta, N., Wu, F., Lee, J.T., and Yushin, G. (2015). Li-ion battery materials: present and future. *Mater. Today* 18, 252–264. <https://doi.org/10.1016/j.mattod.2014.10.040>.
- Pal, A., and Singh, Y.P. (1996). Viscosity in water + ethylene glycol dimethyl, +diethylene glycol dimethyl, +triethylene glycol dimethyl, and +tetraethylene glycol dimethyl ethers at 298.15 K. *J. Chem. Eng. Data* 41, 1008–1011. <https://doi.org/10.1021/je950299e>.
- Rajput, N.N., Qu, X., Sa, N., Burrell, A.K., and Persson, K.A. (2015). The coupling between stability and ion pair formation in magnesium electrolytes from first-principles quantum mechanics and classical molecular dynamics. *J. Am. Chem. Soc.* 137, 3411–3420. <https://doi.org/10.1021/jacs.5b01004>.
- Reinsberg, P., Abd-El-Latif, A.E.A.A., and Baltruschat, H. (2018). Investigation of the complex influence of divalent cations on the oxygen reduction reaction in aprotic solvents. *Electrochim. Acta* 273, 424–431. <https://doi.org/10.1016/j.electacta.2018.03.123>.
- Reinsberg, P., Bondue, C., and Baltruschat, H. (2016). Mechanistic investigation of the oxygen reduction in magnesium ion-containing dimethyl sulfoxide. *Electrochim. Acta* 200, 214–221. <https://doi.org/10.1016/j.electacta.2016.03.157>.
- Sa, N., Pan, B., Saha-Shah, A., Hubaud, A.A., Vaughey, J.T., Baker, L.A., Liao, C., and Burrell, A.K. (2016). Role of chloride for a simple, non-Grignard Mg electrolyte in ether-based solvents. *ACS Appl. Mater. Interfaces* 8, 16002–16008. <https://doi.org/10.1021/acsami.6b03193>.
- Schwenke, K.U., Meini, S., Wu, X., Gasteiger, H.A., and Piana, M. (2013). Stability of superoxide radicals in glyme solvents for non-aqueous Li–O<sub>2</sub> battery electrolytes. *Phys. Chem. Chem. Phys.* 15, 11830. <https://doi.org/10.1039/c3cp51531a>.
- Scott, D.W. (1970). Tetrahydrofuran: vibrational assignment, chemical thermodynamic properties, and vapor pressure. *J. Chem. Thermodyn.* 2, 833–837. [https://doi.org/10.1016/0021-9614\(70\)90026-1](https://doi.org/10.1016/0021-9614(70)90026-1).
- Shiga, T., Hase, Y., Kato, Y., Inoue, M., and Takechi, K. (2013). A rechargeable non-aqueous Mg–O<sub>2</sub> battery. *Chem. Commun.* 49, 9152. <https://doi.org/10.1039/c3cc43477j>.
- Shiga, T., Hase, Y., Yagi, Y., Takahashi, N., and Takechi, K. (2014). Catalytic cycle employing a TEMPO–anion complex to obtain a secondary Mg–O<sub>2</sub> battery. *J. Phys. Chem. Lett.* 5, 1648–1652. <https://doi.org/10.1021/jz506002r>.
- Shimokawa, K., Matsumoto, H., and Ichitsubo, T. (2018). Solvation-structure modification by concentrating Mg(TFSA)<sub>2</sub>–MgCl<sub>2</sub>–triglyme ternary electrolyte. *J. Phys. Chem. Lett.* 9, 4732–4737. <https://doi.org/10.1021/acs.jpcllett.8b02209>.
- Shterenberg, I., Salama, M., Yoo, H.D., Gofer, Y., Park, J.-B., Sun, Y.-K., and Aurbach, D. (2015). Evaluation of (CF<sub>3</sub>SO<sub>2</sub>)<sub>2</sub>N<sup>−</sup> (TFSI) based electrolyte solutions for Mg batteries. *J. Electrochem. Soc.* 162, A7118–A7128. <https://doi.org/10.1149/2.0161513jes>.
- Smith, J.G., Naruse, J., Hiramatsu, H., and Siegel, D.J. (2016). Theoretical limiting potentials in Mg/O<sub>2</sub> batteries. *Chem. Mater.* 28, 1390–1401. <https://doi.org/10.1021/acs.chemmater.5b04501>.
- Tutasaus, O., Mohtadi, R., Arthur, T.S., Mizuno, F., Nelson, E.G., and Sevryugina, Y.V. (2015). An efficient halogen-free electrolyte for use in rechargeable magnesium batteries. *Angew. Chem.* 127, 8011–8015. <https://doi.org/10.1002/ange.201412202>.
- Tutasaus, O., Mohtadi, R., Singh, N., Arthur, T.S., and Mizuno, F. (2017). Study of electrochemical phenomena observed at the Mg metal/electrolyte interface. *ACS Energy Lett.* 2, 224–229. <https://doi.org/10.1021/acsenerylett.6b00549>.
- Vardar, G., Nelson, E.G., Smith, J.G., Naruse, J., Hiramatsu, H., Bartlett, B.M., Sleightholme, A.E.S., Siegel, D.J., and Monroe, C.W. (2015). Identifying the discharge product and reaction pathway for a secondary Mg/O<sub>2</sub> battery. *Chem. Mater.* 27, 7564–7568. <https://doi.org/10.1021/acs.chemmater.5b03608>.
- Vardar, G., Smith, J.G., Thompson, T., Inagaki, K., Naruse, J., Hiramatsu, H., Sleightholme, A.E.S., Sakamoto, J., Siegel, D.J., and Monroe, C.W. (2016). Mg/O<sub>2</sub> battery based on the magnesium–aluminum chloride complex (MACC) electrolyte. *Chem. Mater.* 28, 7629–7637. <https://doi.org/10.1021/acs.chemmater.6b02488>.
- Wang, H.F., and Xu, Q. (2019). Materials design for rechargeable metal–air batteries. *Matter* 1, 565–595. <https://doi.org/10.1016/j.matt.2019.05.008>.
- Wang, Z.L., Xu, D., Xu, J.J., and Zhang, X.B. (2014). Oxygen electrocatalysts in metal–air batteries: from aqueous to nonaqueous electrolytes. *Chem. Soc. Rev.* 43, 7746–7786. <https://doi.org/10.1039/c3cs60248f>.
- Wetteland, C.L., de Jesus Sanchez, J., Silken, C.A., Nguyen, N.Y.T., Mahmood, O., and Liu, H. (2018). Dissociation of magnesium oxide and magnesium hydroxide nanoparticles in physiologically relevant fluids. *J. Nanoparticle Res.* 20, 215. <https://doi.org/10.1007/s11051-018-4314-3>.
- Wróbel, P., Kubisiak, P., and Eilmes, A. (2020). Quantum-chemical and molecular dynamics investigations of magnesium chloride complexes in dimethoxyethane solutions. *ACS Omega* 5, 12842–12852. <https://doi.org/10.1021/acsomega.0c00594>.
- Yagi, S., Tanaka, A., Ichikawa, Y., Ichitsubo, T., and Matsubara, E. (2014). Effects of water content on magnesium deposition from a Grignard reagent-based tetrahydrofuran electrolyte. *Res. Chem. Intermed.* 40, 3–9. <https://doi.org/10.1007/s11164-013-1449-9>.
- Yoo, H.D., Han, S.D., Bolotin, I.L., Nolis, G.M., Bayliss, R.D., Burrell, A.K., Vaughey, J.T., and Cabana, J. (2017). Degradation mechanisms of magnesium metal anodes in electrolytes based on (CF<sub>3</sub>SO<sub>2</sub>)<sub>2</sub>N<sup>−</sup> at high current densities. *Langmuir* 33, 9398–9406. <https://doi.org/10.1021/acs.langmuir.7b01051>.
- Zhang, T., Tao, Z., and Chen, J. (2014). Magnesium–air batteries: from principle to application. *Mater. Horiz.* 1, 196–206. <https://doi.org/10.1039/c3mh00059a>.
- Zhao-Karger, Z., Liu, R., Dai, W., Li, Z., Diemant, T., Vinayan, B.P., Bonatto Minella, C., Yu, X., Manthiram, A., Behm, R.J., et al. (2018). Toward highly reversible magnesium–sulfur batteries with efficient and practical Mg[B(hfip)<sub>4</sub>]<sub>2</sub> electrolyte. *ACS Energy Lett.* 3, 2005–2013. <https://doi.org/10.1021/acsenerylett.8b01061>.

## STAR★METHODS

## KEY RESOURCES TABLE

REAGENT or RESOURCE	SOURCE	IDENTIFIER
Other		
Mg foil	Alfa Aesar	<a href="https://www.alfa.com/en/catalog/040603/">https://www.alfa.com/en/catalog/040603/</a>
Magnesium chloride powder	Alfa Aesar	<a href="https://www.alfa.com/en/catalog/042850/">https://www.alfa.com/en/catalog/042850/</a>
Platinum on carbon	Alfa Aesar	<a href="https://www.alfa.com/en/catalog/L00469/">https://www.alfa.com/en/catalog/L00469/</a>
Anhydrous diglyme	Sigma Aldrich	<a href="https://www.sigmaaldrich.com/CA/en/product/sial/281662">https://www.sigmaaldrich.com/CA/en/product/sial/281662</a>
Magnesium bis(trifluoromethanesulfonimide)	TCI	<a href="https://www.tcichemicals.com/CA/en/p/M2861">https://www.tcichemicals.com/CA/en/p/M2861</a>
Carbon fiber paper	Toray	<a href="https://www.fuelcellearth.com/fuel-cell-products/toray-paper-060/">https://www.fuelcellearth.com/fuel-cell-products/toray-paper-060/</a>
Software and algorithms		
FactSage™ 8.1	FactSage	<a href="https://www.factsage.com/">https://www.factsage.com/</a>
HSC® Chemistry 9.0	HSC Chemistry	<a href="https://www.hsc-chemistry.com/">https://www.hsc-chemistry.com/</a>

## RESOURCE AVAILABILITY

## Lead contact

Further information and requests for resources, measurement procedures, and data should be directed to the corresponding author, Gisele Azimi ([g.azimi@utoronto.ca](mailto:g.azimi@utoronto.ca)).

## Materials availability

This study did not generate new unique reagents.

## Data and code availability

- There is no original code associated with this work.
- Data reported in this paper will be shared by the [lead contact](#) upon request.
- Any additional information required to reanalyze the data reported in this paper will be available from the [lead contact](#) upon request.

## METHOD DETAILS

Preparation of  $\text{Mg}((\text{CF}_3\text{SO}_2)_2\text{N})_2$ - $\text{MgCl}_2$  in G2 electrolyte

Prior to usage,  $\text{Mg}((\text{CF}_3\text{SO}_2)_2\text{N})_2$  and  $\text{MgCl}_2$  were dried in a vacuum oven at 150°C overnight, whereas G2 was pretreated with molecular sieves for a few days before electrolyte preparation. The electrolyte was prepared by adding 2 mmol of  $\text{Mg}((\text{CF}_3\text{SO}_2)_2\text{N})_2$  and 1 mmol of  $\text{MgCl}_2$  into 4 g of G2 (Mg salt concentration: 0.5 m  $\text{Mg}((\text{CF}_3\text{SO}_2)_2\text{N})_2$  + 0.25 m  $\text{MgCl}_2$ ) in an Ar-filled glovebox ( $\text{O}_2$  and  $\text{H}_2\text{O}$  < 1 ppm). The mixture was then magnetically stirred for more than 48 h until a homogeneous and clear solution was achieved. To further remove moisture contamination, the as-prepared electrolyte was soaked in molecular sieves before use.

## Fabrication of Pt/C on CFP air cathode

Approximately 0.1 g of Pt/C was added into 20 mL of anhydrous ethanol and the mixture was ultrasonicated in a bath sonicator for 2 h. The bath sonicator was filled with ice water to minimize the evaporation of ethanol due to heat generation during sonication. The as-prepared Pt/C-ethanol dispersion was then drop casted onto a piece of CFP (diameter: 1.27 cm) using a micropipette and the electrode was further dried in a vacuum oven at 80°C overnight before use. The total mass of Pt/C was ~0.2 mg (equivalent loading: ~0.16 mg cm<sup>-2</sup>).

### Fabrication of electrochemical cells

All preparations and cell assembly were performed inside an Ar-filled glovebox. The Mg|O<sub>2</sub> coin cell was assembled by stacking a Mg foil (~1 × 1 cm; width × length), a piece of GF/A separator (~1.6 cm in diameter) with an air cathode (either CFP alone or Pt/C on CFP). The Mg metal surface was mechanically scraped with the edge of stainless-steel (SS) spatula to expose a shiny subsurface before cell assembly. Approximately 150 μL of electrolyte was added into each cell. To minimize the contact of the electrolyte with the coin cell's SS terminals, a piece of Mo spacer (~1.6 cm in diameter) and Mo gauze (~1.6 cm in diameter) were sandwiched between the negative electrode/terminal and positive electrode/terminal, respectively (Figure 2A). The as-assembled Mg|O<sub>2</sub> coin cell was then positioned into a Swagelok-type bottle cell and the setup was purged with high-purity O<sub>2</sub> for 30 min. Prior to conducting electrochemical testings, the setup was allowed to rest for 10 h to saturate the electrolyte with O<sub>2</sub>. Potential leakage areas of the bottle cell were thoroughly wrapped in polytetrafluoroethylene thread in combination with Parafilm® to prevent exchange of gases with the ambient environment during testing.

Linear sweep voltammetry (LSV) was conducted to study the electrochemical stability of Mg((CF<sub>3</sub>SO<sub>2</sub>)<sub>2</sub>N)<sub>2</sub>-MgCl<sub>2</sub> in G2 electrolyte. Glassy carbon was utilized as the working electrode, Pt as the counter electrode, and Mg immersed in the same electrolyte was treated as the quasi-reference electrode. The same setup was used to investigate Mg electrodeposition/stripping using cyclic voltammetry (CV). To evaluate the Mg electrodeposition/stripping potentials across various current densities, a symmetrical Mg|Mg coin cell were prepared. Molybdenum spacers and Whatman GF/A were utilized as the current collectors and separator, respectively. Similarly, Mg metal surface was mechanically scraped prior to cell assembly.

### Electrochemical testings and characterization

Galvanostatic cycling tests were conducted using a multichannel battery tester (CT-4008, Neware). The discharge/charge current density for the long-term cyclability test was set at 100 mA g<sub>Pt/C</sub><sup>-1</sup> and the cut-off capacity was 500 mAh g<sub>Pt/C</sub><sup>-1</sup>. Prior to conducting full discharge-charge test, the cell was galvanostatically cycled at 100 mA g<sub>Pt/C</sub><sup>-1</sup> (cut-off capacity: 500 mAh g<sub>Pt/C</sub><sup>-1</sup>) for a few cycles to stabilize the cell. Voltammetry and electrochemical impedance spectroscopy (EIS) measurements were performed using a VersaSTAT 3™ potentiostat (Princeton Applied Research). X-ray photoelectron spectroscopy (XPS) analysis was collected on an Escalab250Xi spectrometer with an Mg (Kα) source. Time-of-flight secondary ion mass spectroscopy (ToF-SIMS) analysis was conducted on ToF-SIMS IV instrument from ION-TOF Germany. The primary ion beam used was Bi<sub>3</sub><sup>2+</sup> at 30 keV. Electron microscopic images were acquired using a scanning electron microscope (SEM; Hitachi SU5000) and/or a transmissional electron microscope (TEM; Thermo Scientific Talos 200X) equipped with an energy dispersive spectrometer (EDS). X-ray diffraction (XRD) was performed using Rigaku Miniflex 600 X-ray diffractometer with Cu Kα1 radiation (0.1541 nm) in the range of 20–90° (2θ). Fourier transformation mass spectra (FTMS) of the electrolyte and MgO-equilibrated electrolyte solutions were acquired using electrospray ionization (ESI) on an Orbitrap mass spectrometer (Thermo Q Exactive; Thermo Fisher Scientific) via direct infusion using coated (3AP) borosilicate PicoTip emitters (Econo12, NewObjective) using a nano electrospray ionization source.

All solid specimens were thoroughly rinsed in fresh G2 and were thoroughly dried before characterization. All preparations and cell disassembly were performed inside an Ar-filled glovebox and the samples were kept in airtight containers during transfer process.

### Calculations of theoretical E<sub>AM</sub>

In general, the specific cell-level capacity (Q<sub>cell</sub>) of any battery system can be expressed as (Kasavajjula et al., 2007):

$$Q_{\text{cell}} = \frac{1}{\left(\frac{1}{Q_a}\right) + \left(\frac{1}{Q_c}\right) + \left(\frac{1}{Q_m}\right)} \quad (\text{Equation 2})$$

where Q<sub>a</sub> and Q<sub>c</sub> are the specific capacities of the anode and the cathode (either in mAh g<sup>-1</sup> or interchangeably, Ah kg<sup>-1</sup>), respectively. The term 1/Q<sub>m</sub> represents the contribution from non-electrochemically active components such as current collector, binder, battery-package materials, etc. Given the term 1/Q<sub>m</sub> is remarkably dependent on the cell design and chemistry, (Betz et al., 2019) the contribution of 1/Q<sub>m</sub> is neglected for simplification (where 1/Q<sub>m</sub> ≈ 0), and Equation 2 can be further simplified to:

$$Q_{\text{cell}} = Q_{\text{AM}} \approx \frac{Q_a Q_c}{Q_a + Q_c} \quad (\text{Equation 3})$$

$Q_{\text{AM}}$  is defined as the achievable specific capacity at the active material level.

The theoretical  $Q_a$  and  $Q_c$  can be calculated using Faraday's law of electrolysis:

$$Q_{i(\text{; a,c})} = \frac{Fz_i}{M_i} \quad (\text{Equation 4})$$

where  $F$  is the Faraday constant ( $F = 26801.4 \text{ mAh g}^{-1}$ ),  $z_i$  is the number of moles of electrons transferred (depends on the overall reaction involved), and  $M_i$  is the molar equivalent mass of reactant(s) involved (in  $\text{g mol}^{-1}$ ).

By relating  $Q_{\text{AM}}$  with the theoretical/equilibrium cell potential ( $V_{\text{cell}}$ ), the theoretical specific energy at the active material level ( $E_{\text{AM}}$ ) can be expressed as:

$$E_{\text{AM}} = \left( \frac{Q_a Q_c}{Q_a + Q_c} \right) V_{\text{cell}} = Q_{\text{AM}} V_{\text{cell}} \quad (\text{Equation 5})$$

For any battery system,  $V_{\text{cell}}$  can be calculated from the reaction free energy ( $\Delta G_r$ ) following:

$$V_{\text{cell}} = -\left( \frac{\Delta G_r}{z_i F} \right) \quad (\text{Equation 6})$$

$\Delta G_r$  presented in [Table S1](#) was determined by HSC® Chemistry 9 at 25°C.